The EMBO Journal (2012) 31, 1123–1133 | © 2012 European Molecular Biology Organization | All Rights Reserved 0261-4189/12
www.embojournal.org

THE EMBO JOURNAL

STIM1 is required for attenuation of PMCA-mediated Ca^{2+} clearance during T-cell activation

Michael F Ritchie[1], Elsie Samakai and Jonathan Soboloff*

Department of Biochemistry, Temple University School of Medicine, Philadelphia, PA, USA

T-cell activation involves a complex signalling cascade uniquely dependent on elevated cytosolic Ca^{2+} levels. Further, the spatiotemporal characteristics of this Ca^{2+} signal play a critical role in this process via selective activation of transcription factors. In T cells, store-operated Ca^{2+} entry (SOCe) is the primary Ca^{2+} influx pathway; however, cytosolic Ca^{2+} concentration depends upon the balance between Ca^{2+} influx and extrusion. The plasma membrane Ca^{2+} ATPase (PMCA) has previously been identified as a critical player in Ca^{2+} clearance in T cells. Here, we provide data revealing both functional and physical links between the activation of stromal interacting molecule 1 (STIM1) and PMCA-mediated Ca^{2+} clearance. Due to the ubiquitous expression of both STIM1 and PMCA, these findings have wide-ranging implications for Ca^{2+} signalling in multiple cell types.

The EMBO Journal (2012) **31,** 1123–1133. doi:10.1038/emboj.2011.495; Published online 13 January 2012
Subject Categories: membranes & transport; immunology
Keywords: calcium; lymphocyte; PMCA; STIM1; T cell

Introduction

T-cell activation involves increased cytokine (e.g., IL-2) production and secretion, clonal expansion and differentiation (Oh-hora, 2009; Reicher and Barda-Saad, 2010). The critical transcription factor mediating this change is nuclear factor of activated T cells (NFAT) (Oh-hora and Rao, 2008). However, NFAT activity is uniquely dependent on cytosolic Ca^{2+} signals (Di Capite *et al*, 2009); extended elevations of cytosolic Ca^{2+} concentration ($[Ca^{2+}]_c$) lead to dephosphorylation of NFAT via calcineurin and transport into the nucleus. It is now generally accepted that the stromal interacting molecule 1 (STIM1)-dependent and Ca^{2+}-selective channel Orai1 is the primary source of Ca^{2+} influx during T-cell activation needed to support NFAT activation (Oh-Hora *et al*, 2008; Deng *et al*, 2009; Hogan *et al*, 2010). However, plasma membrane Ca^{2+} ATPase (PMCA) also plays a critical role as a regulator of cytosolic Ca^{2+} dynamics in T cells (Lewis, 2001). Hence, PMCA provides the sole mechanism for cellular Ca^{2+} extrusion in this cell type and has previously been shown to functionally associate with store-operated Ca^{2+} channels in plasma membrane microdomains (Bautista and Lewis, 2004). However, the relationship between STIM1, Orai1 and PMCA has not been determined.

*Corresponding author. Department of Biochemistry, Temple University School of Medicine, 3440 North Broad Street, Philadelphia, PA 19140, USA. Tel.: +1 215 707 6567; Fax: +1 215 707 7536;
E-mail: soboloff@temple.edu
[1]Present address: Brigham and Women's Hospital, New Research Building 636, 77 Avenue Louis Pasteur, Boston, MA 02115, USA

Received: 6 July 2011; accepted: 12 December 2011; published online: 13 January 2012

Results and discussion

Cytosolic Ca^{2+} clearance is reduced in activated T cells

We have previously shown that STIM1 expression is controlled by the transcription factor early growth response 1 (EGR1) (Ritchie *et al*, 2010). To assess EGR1-dependent modulation of long-term Ca^{2+} dynamics, we examined the expression of several Ca^{2+} homeostatic proteins after induction of EGR1 expression in Jurkat T cells by stimulating T-cell receptor (TCR) cross-linking using the lectinphytohemagglutinin (PHA). As expected, EGR1 was upregulated within 1 h of activation, rapidly followed by increased expression of both STIM1 and STIM2 (Figure 1A). Unexpectedly, expression of both PMCA4 (the major PMCA isoform expressed in Jurkat cells (Caride *et al*, 2001)) and PMCA1 increased with T-cell activation (Figure 1A and B). To assess the functional implications of these PHA-mediated changes in STIM and PMCA expression, we compared cytosolic Ca^{2+} entry and clearance in Jurkat cells before and 2 h after activation with either PHA or the monoclonal TCR antibody OKT3 (Figure 1C). This was achieved in cells treated with 2 μM thapsigargin (Tg) in a Ca^{2+}-free solution to deplete ER Ca^{2+} stores via inhibition of the Sarco-Endoplasmic Ca^{2+}/ATPase (SERCA). This served a dual purpose; under these conditions, store-operated Ca^{2+} entry (SOCe) measurement was followed by examination of Ca^{2+} clearance in the absence of SERCA activity (analogous studies performed in this cell type identified PMCA as the major mediator of $[Ca^{2+}]_c$ extrusion in T cells in the absence of SERCA activity (Bautista *et al*, 2002; Bautista and Lewis, 2004)). Measurement of the change in $[Ca^{2+}]_c$ after increasing extracellular Ca^{2+} concentration ($[Ca^{2+}]_e$) to 1 mM revealed a modest increase in SOCe after PHA-induced activation (Figure 1C and D), presumably due to increased STIM1 expression. However, quite unexpectedly, we found a substantial increase in the period required for $[Ca^{2+}]_c$ to reach basal levels after the removal of extracellular Ca^{2+} (Figure 1C), despite the apparent increase in PMCA expression. To determine if this finding was generally applicable to T cells, experiments were also performed in primary murine thymocytes (Supplementary Figure S1A and B) and CEM391 T cells (Supplementary Figure S1C and D). Similar to Jurkat T cells, PMCA-mediated Ca^{2+} clearance was compromised to a similar degree in either cell type, despite PHA-induced elevation of PMCA expression.

To quantify differences in $[Ca^{2+}]_c$ clearance, non-linear regression analyses of the $[Ca^{2+}]_c$ clearance curves were performed, using either single or dual exponential decay where appropriate based on curve fit analysis. The initial time point for each fit was the first time point recorded

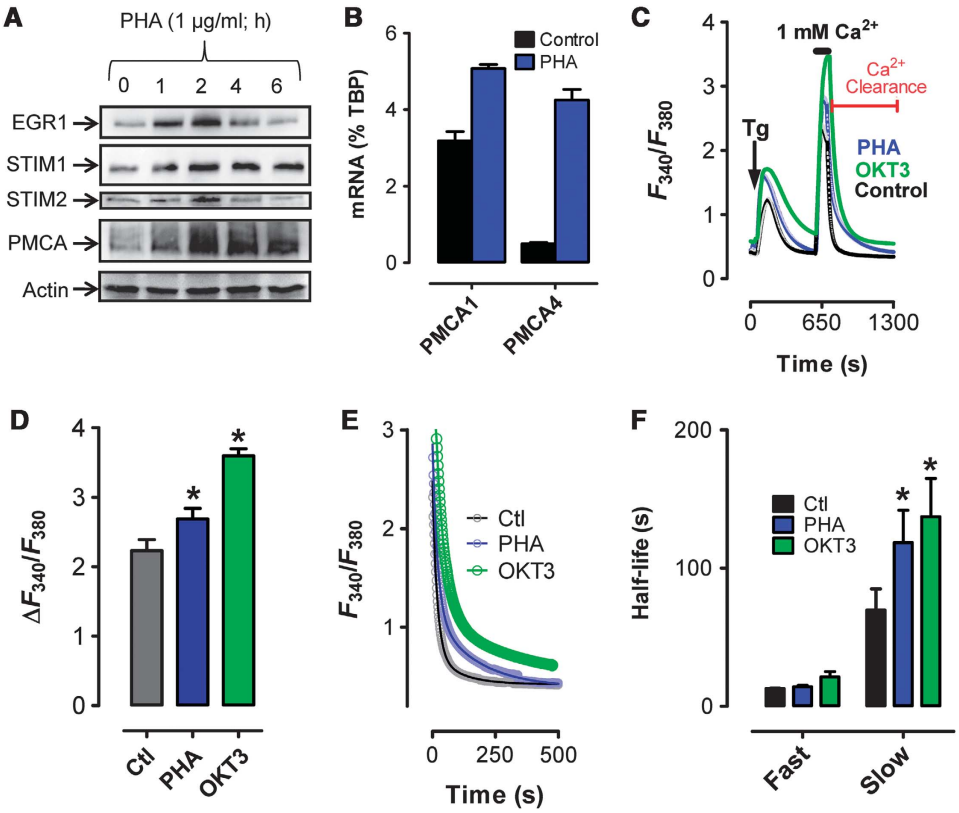

Figure 1 PHA-induced remodelling of cytosolic Ca^{2+} homeostasis. (**A**) Jurkat T cells were treated with 1 μg/ml PHA, 100 nM OKT3 or vehicle (H_2O) before cell lysis at the indicated time points and analysed by western blot as depicted. (**B**) Jurkat T cells were treated with PHA or vehicle for 2 h before cell lysis, RNA extraction and analysis of PMCA1 and PMCA4 expression by qPCR; values normalized to TATA-binding protein (TBP). (**C**) Jurkat T cells were treated with PHA or vehicle for 2 h before loading with Fura-2 and depleting ER Ca^{2+} stores with Tg (2 μM) in the absence of $[Ca^{2+}]_e$. Subsequent elevation of $[Ca^{2+}]_e$ to 1 mM led to elevated $[Ca^{2+}]_c$; upon reaching its peak, $[Ca^{2+}]_e$ was again removed to monitor $[Ca^{2+}]_c$ clearance. (**D**) The magnitude of SOCe was assessed by subtracting basal F_{340}/F_{380} from the maximum F_{340}/F_{380} in Jurkat cells treated with vehicle, PHA or OKT3. (**E**, **F**) $[Ca^{2+}]_c$ clearance was determined from the data depicted in the last part of the trace from (**C**). (**E**) Symbols represent individual data points while the solid lines are interpolated from two-phase, non-linear regression analysis (Ctl, $R^2=0.85$, $n=10$; PHA $R^2=0.91$, $n=9$; OKT3 $R^2=0.90$, $n=3$). All traces are representative of multiple experiments of $[Ca^{2+}]_c$ signals assessed in Jurkat cells treated with PHA, OKT3 or vehicle. (**F**) Half-lives calculated from the curve depicted in (**E**) are depicted and compared. Significant differences were determined using the extra sum of squares *F*-test with * denoting statistically significant differences ($P<0.05$).

immediately after the removal of extracellular Ca^{2+} (Figure 1C). Under these conditions, $[Ca^{2+}]_c$ clearance followed a dual exponential decay pattern (curve fits shown in Figure 1E) in agreement with previously published findings (Bautista *et al*, 2002; Bautista and Lewis, 2004). Intriguingly, while little difference in the initial fast decay phase was observed, the secondary slow phase was significantly attenuated after PHA- or OKT3-mediated T-cell activation (Figure 1E and F; Supplementary Table SI). Additionally, there was a two-fold increase in the amplitude at which the secondary, slow phase of decay begins (Figure 1E; Supplementary Table SI). In the light of this remarkable and wholly unexpected finding, the focus of our investigation shifted towards ascertaining mechanism(s) responsible for attenuation of $[Ca^{2+}]_c$ clearance during T-cell activation.

Mitochondria-dependent and -independent components of Ca^{2+} clearance

A critical role for mitochondria as modulators of Ca^{2+} clearance during T-cell activation has previously been defined (Quintana *et al*, 2006, 2007; Schwindling *et al*, 2010). Therefore, we assessed the possibility that differences in mitochondrial Ca^{2+} dynamics were contributing to the attenuation of $[Ca^{2+}]_c$ clearance during T-cell activation. First, we reduced the time period that 1 mM $[Ca^{2+}]_e$ was added before assessing Ca^{2+} clearance; this was done to minimize differences in $[Ca^{2+}]_m$ loading by removing $[Ca^{2+}]_e$ and assessing $[Ca^{2+}]_c$ clearance before differences in $[Ca^{2+}]_c$ became apparent. Accordingly, we found that adding $[Ca^{2+}]_e$ for ~45 s led to similar increases in cytosolic and mitochondrial Ca^{2+} levels (Figure 2A and B). We then assessed clearance of both cytosolic and mitochondrial Ca^{2+} before and after PHA-induced activation using this protocol. Interestingly, impaired Ca^{2+} clearance was observed in both the cytosol (Figure 2A) and the mitochondria (Figure 2B) in activated T cells despite the absence of any apparent difference in total mitochondria Ca^{2+} loading (Figure 2B). In the absence of any difference in mitochondrial Ca^{2+} loading, the most likely cause of a difference in mitochondrial Ca^{2+} release would be a failure of $[Ca^{2+}]_c$ to return to basal levels for mitochondrial-independent reasons, such as attenuated PMCA activity. Consistent with this concept, inhibition of PMCA function by incubation in 3 mM La^{3+} dramatically delayed the release of mitochondrial Ca^{2+} (Figure 2C). Further support for the existence of a mitochondrial-independent component of PHA-induced inhibition of $[Ca^{2+}]_c$ clearance was obtained using the highly specific mitochondrial

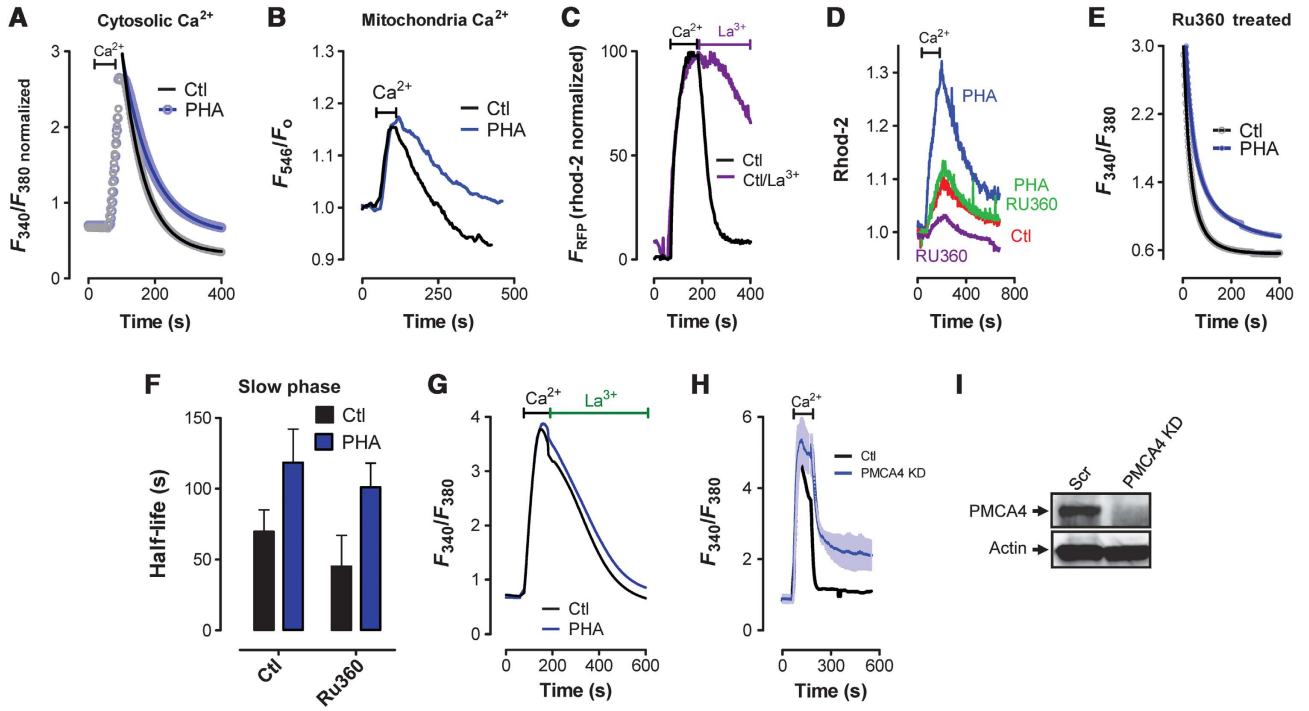

Figure 2 Mitochondrial-independent control of $[Ca^{2+}]_c$ clearance. (**A**–**H**) Jurkat T cells were treated with PHA or vehicle and loaded with rhod-2 for 1 h before loading with fura-2 for 1 h and depleting ER Ca^{2+} stores with Tg (2 μM) in the absence of $[Ca^{2+}]_e$ (not depicted). Once $[Ca^{2+}]$ had returned to baseline, $[Ca^{2+}]_e$ was elevated to 1 mM; upon reaching peak $[Ca^{2+}]$, $[Ca^{2+}]_e$ was again removed. ((**A**, **B**) $[Ca^{2+}]_c$ (**A**) and $[Ca^{2+}]$m (**B**) Ca^{2+} clearance is assessed in resting and PHA-treated cells after $[Ca^{2+}]_e$ is added for 45 s. Cytosolic baseline Ca^{2+} levels in both Ctl and PHA-treated cells are normalized to illustrate clearly the similarity in the change in $[Ca^{2+}]_m$. (**C**) Elevation of $[Ca^{2+}]_e$ to 1 mM in Tg-pretreated T cells led to elevated $[Ca^{2+}]_m$; $[Ca^{2+}]_m$ clearance was then assessed in the presence (purple trace) or absence (black trace) of 3 mM extracellular La^{3+} added when $[Ca^{2+}]_e$ was again removed. Cytosolic Ca^{2+} levels are normalized. (**D**, **E**) One hour prior to performing Ca^{2+} measurements, cells were loaded with RU360 (10 μM) followed by measurements of both mitochondrial (**D**) and $[Ca^{2+}]_c$ (**E**). (**F**) Half-lives calculated from the curve depicted in (**E**) are depicted and compared. (**G**) Elevation of $[Ca^{2+}]_e$ to 1 mM in Tg-pretreated T cells led to elevated $[Ca^{2+}]_c$; $[Ca^{2+}]_c$ clearance was then assessed in the presence of 3 mM extracellular La^{3+} starting from the point that $[Ca^{2+}]_e$ was again removed. (**H**, **I**) Jurkat cells were transfected with siRNA targeting PMCA4 48 h prior to assessing $[Ca^{2+}]_c$ clearance (**H**) and the expression of PMCA4 and actin by western analysis (**I**).

uniporter inhibitor RU360 (Baughman *et al*, 2011). As depicted in Figure 2D, Ru360 dramatically decreased mitochondrial Ca^{2+} loading in both control and PHA-treated cells. However, this had no significant effect on $[Ca^{2+}]_c$ clearance (Figure 2E), with PHA-induced activation still resulting in a significant delay in the slow phase of $[Ca^{2+}]_c$ clearance (Figure 2F). Finally, we assessed the potential involvement of PMCA as a mediator of attenuated $[Ca^{2+}]_c$ clearance during T-cell activation. Interestingly, no PHA-dependent differences in the rate of $[Ca^{2+}]_c$ clearance were observed after PMCA inhibition via the addition of La^{3+}, despite notable differences in maximal $[Ca^{2+}]_e$ and a dramatic alteration in the shape of the $[Ca^{2+}]_c$ clearance curve (Figure 2G). We also examined $[Ca^{2+}]_c$ clearance rates in cells transfected with PMCA4 siRNA to see if this manipulation might mimic the effect of PHA. We found that PMCA4 knockdown dramatically inhibited the second phase of $[Ca^{2+}]_c$ clearance (Figure 2H and I). Considered collectively, these findings provide strong support for the notion that, in addition to any role played by mitochondria as modulators of $[Ca^{2+}]_c$ clearance during T-cell activation, PMCA activity may be independently modulated during this process.

In an effort to identify potential causes of reduced PMCA activity in activated T cells, we examined previously identified PMCA regulatory mechanisms. Prior studies have shown that Ca^{2+} modulates PMCA activity with a reversal time constant of ~10 min (Bautista *et al*, 2002). However, increasing the resting period from ~7 to 14 min between the Tg-induced Ca^{2+} elevation and the assessment of $[Ca^{2+}]_c$ clearance had no effect on PMCA inhibition induced by T-cell activation (data not shown). Further, since PHA-induced TCR activation also initiates Ca^{2+} influx, cells were treated with PHA in the presence of 1.5 mM EGTA (setting $[Ca^{2+}]_e$ at 300 μM) thereby reducing PHA-induced Ca^{2+} influx. However, this also had no effect on the ability of PHA to inhibit PMCA activity (data not shown), indicating that PHA-induced $[Ca^{2+}]_c$ elevation cannot account for PHA-induced inhibition of PMCA activity.

STIM1 reduces PMCA-mediated Ca^{2+} clearance via physical interaction

In addition to PMCA, both STIM1 and STIM2 expression were increased after T-cell activation (Figure 1A). In order to assess the contribution of these proteins in control of $[Ca^{2+}]_c$ clearance during T-cell activation, Jurkat cells were transfected with YFP-tagged STIM1 (YFP–S1) or STIM2 (YFP–S2) and $[Ca^{2+}]_c$ clearance rates were assessed. Analysis of STIM1 expression levels revealed that YFP–S1 was expressed at levels similar to endogenous STIM1 (Supplementary Figure S2A) and only marginally increased SOCe (Supplementary Figure S2B). Remarkably, we found significant differences in $[Ca^{2+}]_c$ clearance rate in cells expressing YFP–S1 in a manner similar to PHA or OKT3-activated cells (Figure 1F).

Hence, upon removal of $[Ca^{2+}]_e$, $[Ca^{2+}]_c$ returned to basal levels following a two-phase exponential decay pattern (Figure 3A) and while there were no significant differences in the fast decay phase, the slow phase of $[Ca^{2+}]_c$ clearance in YFP–S1 overexpressing cells was significantly attenuated and developed from a higher amplitude (Figure 3A and B; Supplementary Table SI). Further, activation of YFP–S1 expressing cells with PHA had no additive effect on reducing $[Ca^{2+}]_c$ clearance rates (Figure 3A and B). Finally, we examined the effect of YFP–S2 overexpression on $[Ca^{2+}]_c$ clearance rates, finding no significant differences with control for either the fast or slow decay $[Ca^{2+}]_c$ clearance rates (Figure 3A and B).

We also characterized physical interactions between STIM1 and PMCA under endogenous expression levels. Immunoprecipitation using pan-PMCA (Figure 3C) or STIM1 (Figure 3D) antibodies revealed significant interactions between STIM1 and PMCA under resting conditions; this interaction was only moderately enhanced by PHA-induced activation. This may provide further evidence of a critical role for elevated expression of both STIM1 and PMCA during T-cell activation (Figure 1A), since their level of expression seems to influence the amount of interaction. Note that PMCA4-specific antibodies demonstrate that STIM1 specifically interacts with the PMCA4 isoform (Figure 3D). We then examined the cytolocalization of STIM1 and PMCA in activated cells. As expected given prior reports (Barr *et al*, 2008; Lioudyno *et al*, 2008), STIM1 polarized dramatically after PHA activation towards the area of the cell where a fluorescently labelled PHA also accumulates (Figure 3E), consistent with the formation of an immunological synapse (IS); less obvious was that GFP–PMCA4 was similarly localized to the site where a similarly fluorescently labelled PHA accumulates upon activation (Figure 3E). Finally, we examined the degree of colocalization between STIM1 and PMCA both before and after PHA-induced activation (Figure 3F). Intriguingly, there was only minimal colocalization prior to activation, yet stark colocalization of STIM1 and PMCA after activation. Furthermore, the addition of Tg to PHA-treated cells had no effect on the degree of STIM1/PMCA colocalization (data not shown) supporting the contention that this colocalization is stable and not affected

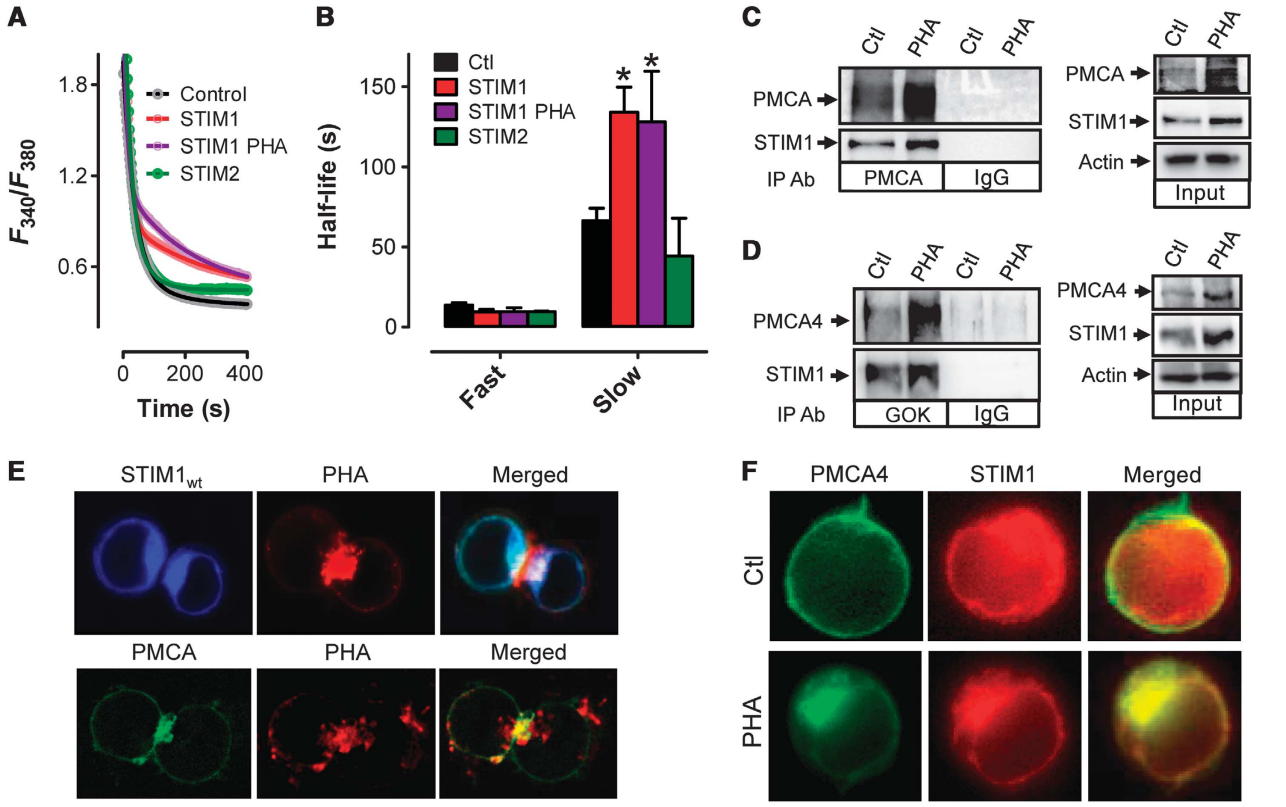

Figure 3 STIM1 inhibits PMCA function via physical interaction at the IS. (**A**) Jurkat T cells were transfected as indicated 48 h before loading with Fura-2 and depleting ER Ca^{2+} stores with Tg (2 μM) in the absence of extracellular Ca^{2+}. Subsequent elevation of $[Ca^{2+}]_e$ to 1 mM led to elevated $[Ca^{2+}]_c$; upon reaching its peak, $[Ca^{2+}]_e$ was again removed to monitor $[Ca^{2+}]_c$ clearance. Note that only the last part of each curve is depicted due to space considerations. $[Ca^{2+}]_c$ clearance rates were analysed by two-phase, non-linear regression analysis. Symbols represent individual data points while the solid lines are interpolated from (YFP, $R^2 = 0.85$, $n = 10$; STIM1, $R^2 = 0.81$, $n = 8$; STIM1 PHA, $R^2 = 0.90$, $n = 5$; STIM2, $R^2 = 0.93 \pm 0.02$, $n = 3$). (**B**) Half-lives obtained from non-linear regression analysis of experiments depicted in (**A**). (**C**, **D**) Jurkat cells were treated with PHA or vehicle for 2 h followed by lysis, and immunoprecipitation (left) with PMCA (**C**) or STIM1 (**D**) antibodies followed by western analysis. (Right) In all, 25 μg of total protein was loaded to determine relative expression levels of STIM1 and PMCA prior to immunoprecipitation. Actin was used as a loading control. (**E**) Jurkat cells were transfected with CFP–STIM1 (upper) or GFP–PMCA (lower). In all, 48 h after transfection, cells were treated with Alexafluor594-conjugated PHA for 2 h, mounted on a cover slip and STIM1 and PHA localization was assessed. (**F**) Jurkat cells were cotransfected with mCherry-STIM1 and GFP–PMCA. In all, 48 h after transfection, cells were placed on cover slips with PHA or vehicle (Ctl) and 2 h later, STIM1 and PMCA cellular localization was assessed. Tg was added to PHA-treated cells and STIM1/PMCA cellular localization was assessed 10 min later. Significant differences were determined using the extra sum of squares *F*-test with * denoting statistically significant differences ($P < 0.05$).

by ER store depletion. Hence, PHA-induced increased interaction between STIM1 and PMCA may, at least in part, result from increased physical association due to enhanced physical proximity associated with the activation process.

Identification of critical STIM1 domains regulating PMCA-mediated Ca^{2+} clearance

We then attempted to determine which cytosolic STIM1 components were responsible for attenuation of PMCA-mediated $[Ca^{2+}]_c$ clearance by examining a series of STIM1 truncation mutants (Figure 4A). We found that cells expressing a STIM1 construct lacking the lysine-rich domain ($STIM1_{\Delta K}$) exhibited greatly decreased $[Ca^{2+}]_c$ clearance similar to wild-type STIM1 ($STIM1_{wt}$) (Figure 4B). However, $[Ca^{2+}]_c$ clearance was unaffected by expressing a STIM1 construct truncated immediately upstream of the proline-rich region (PRR) ($STIM1_{\Delta 597}$; Figure 4B). Quantification of $[Ca^{2+}]_c$ clearance by fitting data to a two-phase, non-linear regression revealed little difference between $STIM1_{wt}$ and $STIM1_{\Delta K}$; the secondary phase of $[Ca^{2+}]_c$ clearance began from a higher amplitude and decayed at a significantly slower rate (Figure 4C; Supplementary Table SI). However, $[Ca^{2+}]_c$ clearance in cells expressing $STIM1_{\Delta 597}$ exhibited similar characteristics to cells expressing YFP (Figure 4C) despite no differences in the magnitude of SOCe in cells expressing either $STIM1_{wt}$ or $STIM1_{\Delta 597}$ (Figure 4D). Hence, differences in the relative abilities of these two STIM1 moieties to stimulate $[Ca^{2+}]_e$ influx cannot account for differences in

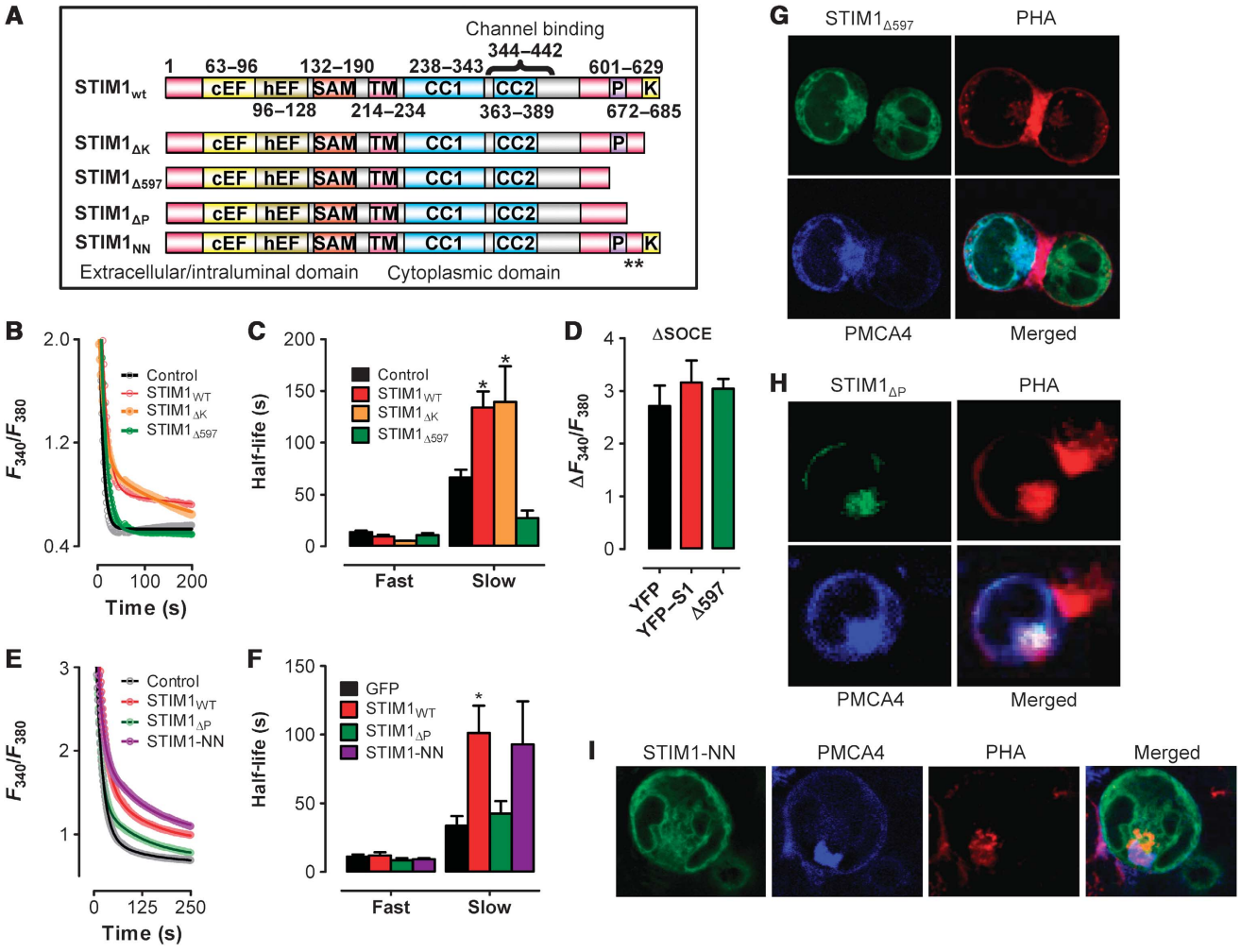

Figure 4 Analysis of STIM1-mediated control of PMCA activation. (**A**) Schematic of the STIM1 constructs used; ** indicates I644N/P645N mutation. (**B**) Jurkat T cells were transfected as indicated 48 h before loading with Fura-2 and depleting ER Ca^{2+} stores with Tg (2 μM) in the absence of extracellular Ca^{2+}. Subsequent elevation of $[Ca^{2+}]_e$ to 1 mM led to elevated $[Ca^{2+}]_c$; upon reaching its peak, $[Ca^{2+}]_e$ was again removed to monitor $[Ca^{2+}]_c$ clearance. Note that only the last part of each curve is depicted due to space considerations. $[Ca^{2+}]_c$ clearance rates were analysed by two-phase, non-linear regression analysis. Symbols represent individual data points while the solid lines are interpolated from one-phase, non-linear regression analysis (YFP, $R^2=0.85$, $n=5$; $STIM1_{wt}$, $R^2=0.81$, $n=8$; $STIM1_{\Delta K}$, $R^2=0.92$, $n=3$; $STIM1_{\Delta 597}$, $R^2=0.91$, $n=3$). (**C**) Half-lives obtained from non-linear regression analyses performed in experiments depicted in (**B**) were analysed by one-way ANOVA. * denotes statistically significant difference ($P<0.05$). (**D**) The magnitude of SOCe reached for cells expressing YFP, $STIM1_{wt}$ or $STIM1_{\Delta 597}$ were calculated by subtracting the basal F_{340}/F_{380} from the maximum F_{340}/F_{380} reached during the application of 1 mM extracellular Ca^{2+}. (**E**) Jurkat T were transfected as indicated and analysed as described for panel (**B**). Curve fits as follows: GFP, $R^2=0.92$, $n=4$; $STIM1_{wt}$, $R^2=0.97$, $n=4$; $STIM1_{\Delta P}$, $R^2=0.97$, $n=4$; STIM1-NN, $R^2=0.97$, $n=4$. (**F**) Half-lives obtained from non-linear regression analyses performed in experiments depicted in (**E**) were analysed by one-way ANOVA. * denotes statistically significant difference ($P<0.05$). (**G–I**) Jurkat cells were transfected with CFP–PMCA4 and $STIM1_{\Delta 597}$ (**G**), $STIM1_{\Delta P}$ (**H**) or STIM1-NN (**I**). At 48 h after transfection, cells were treated with Alexafluor594-conjugated PHA for 2 h, mounted on a cover slip and STIM1 and PHA localization was assessed.

$[Ca^{2+}]_c$ clearance observed in cells expressing $STIM1_{wt}$ versus $STIM1_{\Delta 597}$. To expand on this point, we also examined cells expressing $STIM1_{\Delta 441-448}$, a STIM1 moiety that fails to activate Orai1-mediated Ca^{2+} influx (Wang *et al*, 2010). We found that overexpression of $STIM1_{\Delta 441-448}$ failed to increase Ca^{2+} influx, but impaired $[Ca^{2+}]_c$ clearance (Supplementary Figure S3A) in a manner similar to $STIM1_{wt}$. We also assessed how a constitutively active full-length STIM1 protein affects $[Ca^{2+}]_c$ clearance. We found that the constitutively active $STIM1_{D76A}$ mutant inhibited Ca^{2+} clearance similar to $STIM1_{\Delta 441-448}$ (Supplementary Figure S3B), although in this case, we did observe elevated $[Ca^{2+}]_c$. Finally, we examined the cytolocalization of $STIM1_{\Delta 441-448}$ (Supplementary Figure S3C) and $STIM1_{D76A}$ (Supplementary Figure S3D) after PHA-induced T-cell activation, observing a similar colocalization with CFP–PMCA and PHA independent of these activation mutations. Collectively, these data suggest that the reorganization of STIM1 towards the site of PHA accumulation and the inhibition of PMCA function are independent from STIM1-mediated control of Orai1 activity.

Based on the evidence described in Figure 4B–D, we hypothesized that there may be a domain located on STIM1 between amino acid 597 and 672 (the site of the ΔK truncation) with PMCA modulatory functions. Interestingly, this region of STIM1 has already been shown to contain a PRR with no currently defined role and an EB1-binding motif that binds to the growing ends of microtubules (Grigoriev *et al*, 2008; Honnappa *et al*, 2009). Accordingly, we assessed the contributions of these STIM1 domains towards the attenuation of $[Ca^{2+}]_c$ clearance. This was accomplished utilizing STIM1 constructs exhibiting either deletion of the PRR ($STIM1_{\Delta P}$) or mutations within the EB1-binding motif rendering it incapable of binding microtubules (STIM1-NN; Honnappa *et al*, 2009). We found that cells overexpressing STIM1-NN exhibited a similar reduction in $[Ca^{2+}]_c$ clearance to cells expressing $STIM1_{wt}$ (Figure 4E and F), whereas loss of the PRR greatly attenuated STIM1-mediated inhibition of $[Ca^{2+}]_c$ clearance ($STIM1_{\Delta P}$; Figure 4E and F). Quantification of $[Ca^{2+}]_c$ clearance by fitting data to a two-phase, non-linear regression revealed little difference between $STIM1_{wt}$ and STIM1-NN; the secondary phase of $[Ca^{2+}]_c$ clearance began from a higher amplitude and decayed at a significantly slower rate (Figure 4F; Supplementary Table SI). However, $[Ca^{2+}]_c$ clearance in cells expressing $STIM1_{\Delta P}$ exhibited similar characteristics to cells expressing YFP (Figure 4F; Supplementary Table SI), suggesting that the PRR of STIM1 is critical for attenuation of $[Ca^{2+}]_c$ clearance. Using an Alexafluor594-labelled PHA, we further assessed the ability of $STIM1_{\Delta 597}$, $STIM1_{\Delta P}$ and STIM1-NN to colocalize with PMCA at the site of PHA activation. We found that $STIM1_{\Delta 597}$ (Figure 4G), $STIM1_{\Delta P}$ (Figure 4H) and STIM1-NN (Figure 4I) all localized within close proximity to PMCA and PHA during T-cell activation. Thus, a loss of cellular reorganization dynamics does not account for the lack of effect that $STIM1_{\Delta 597}$ and $STIM1_{\Delta P}$ has on $[Ca^{2+}]_c$ clearance.

We also generated a number of cytosolic STIM1 constructs, none of which could mimic inhibition of PMCA function by full-length STIM1 (data not shown). While we cannot fully account for this finding, we would speculate that anchoring to the ER may be a prerequisite for this phenomenon. A recent investigation identifying a potential role for an ER membrane protein termed Partner-Of-STIM1 (POST) as a mediator of STIM1–PMCA interactions is consistent with this conclusion (Krapivinsky *et al*, 2011).

STIM1 knockdown abrogates activation-induced attenuation of PMCA

To determine if STIM1 is required for PHA-induced attenuation of PMCA-mediated $[Ca^{2+}]_c$ clearance, cells were transfected with scrambled RNA (Scr) or STIM1 siRNA (S1KD). S1KD resulted in a >50% reduction in basal STIM1 expression and totally blocked PHA-induced STIM1 upregulation (Figure 5A). As anticipated, PHA-induced inhibition of $[Ca^{2+}]_c$ clearance was unaffected by transfection with Scr (Figure 5B); the secondary phase of $[Ca^{2+}]_c$ clearance began from a higher amplitude and decayed at a significantly slower rate (Figure 5G; Supplementary Table SI). In contrast, no PHA-mediated inhibition of $[Ca^{2+}]_c$ clearance was observed after S1KD (Figure 5C). However, presumably due to the decrease in $[Ca^{2+}]_c$ attained, $[Ca^{2+}]_c$ clearance followed a single-phase exponential decay pattern (Figure 5H; consistent with Bautista *et al*, 2002). To determine if loss of PHA-mediated inhibition of $[Ca^{2+}]_c$ clearance could be accounted for by either the reduction in maximal $[Ca^{2+}]_c$ or the conversion to a single-phase $[Ca^{2+}]_c$ clearance dynamic, we assessed the ability of the SOCe inhibitor BTP2 to modulate $[Ca^{2+}]_c$ clearance during T-cell activation. Prior studies have defined an IC50 of 300 nM for BTP2 to inhibit SOCe (Ishikawa *et al*, 2003; Zitt *et al*, 2004; He *et al*, 2005), analogous to the 50% reduction in SOCe observed after S1KD. As expected, measurement of SOCe in cells treated with 300 nM BTP2 led to a 50% reduction in SOCe (Figure 5E), which was unaffected by PHA incubation (Figure 5E and F). Irrespective, PHA-mediated inhibition of $[Ca^{2+}]_c$ clearance was still observed in the presence of BTP2 (Figure 5D and H) despite the expected change in the dynamics of $[Ca^{2+}]_c$ clearance to a one-phase decay pattern. Hence, whereas the one-phase versus two-phase $[Ca^{2+}]_c$ clearance relationship appeared to be related to the amount of SOCe, PHA-induced PMCA inhibition was independent of SOCe magnitude. Considered collectively, our data support the possibility that STIM1 itself may be the primary mediator of PHA-induced changes in PMCA activity in the T-cell activation response.

$STIM1_{wt}$ reconstitutes attenuation of PMCA during T-cell activation in S1KD cells

In an effort to assess whether re-expression of STIM1 after STIM1 knockdown could reconstitute PHA-dependent attenuation of PMCA-mediated Ca^{2+} clearance during T-cell activation, Jurkat cells stably expressing STIM1 shRNA (shS1) or an shRNA scrambled sequence (shCtl) were generated. This was done by transfecting cells with the shRNA constructs, selecting with puromycin and cloning to identify subpopulations exhibiting significant loss of STIM1 expression. Our chosen shS1-expressing clone exhibited an ~50% reduction in STIM1 protein levels in shS1-expressing cells compared with shCtl-expressing cells and significantly attenuated PHA-induced STIM1 upregulation (Figure 6A). As expected, shCtl-expressing cells exhibited typical PHA-mediated inhibition of both the rate and initial amplitude of the second $[Ca^{2+}]_c$ clearance phase (Figure 6B). Further, similar to what was observed after transient knockdown of STIM1 using siRNA, PHA-dependent attenuation of PMCA-mediated Ca^{2+} clearance was not observed in shS1-expressing cells (Figure 6C). However,

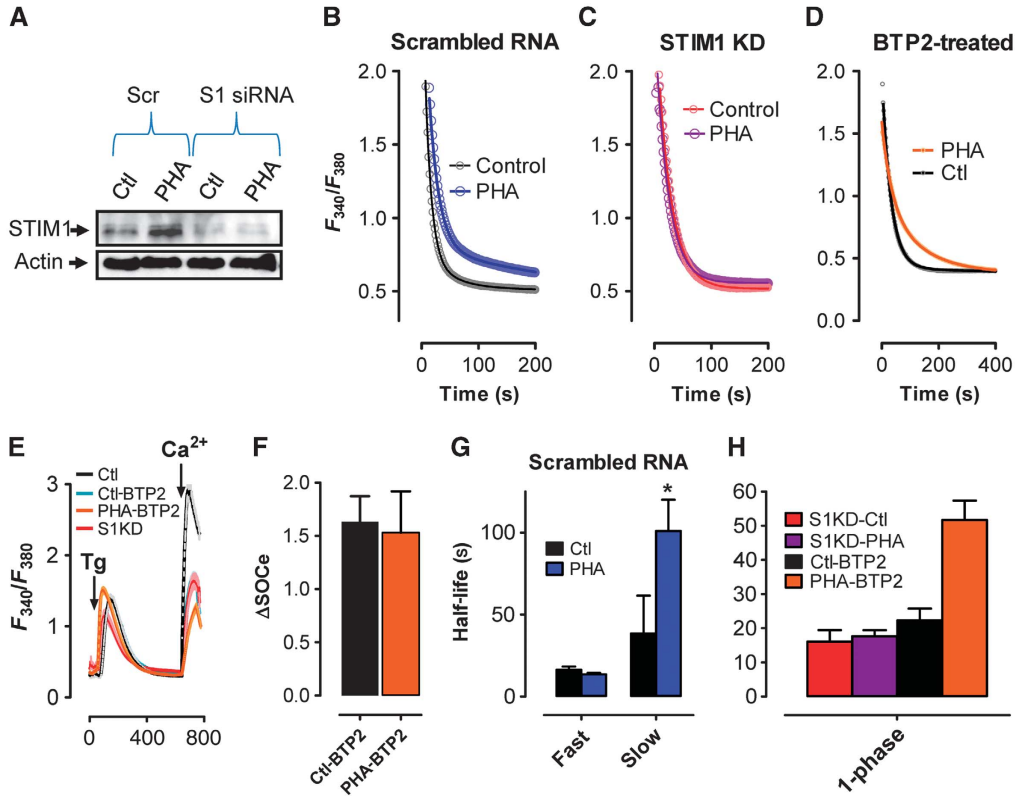

Figure 5 STIM1 knockdown abrogates PMCA attenuation during T-cell activation. (**A**) Jurkat cells were transfected with scrambled siRNA or STIM1-targeted siRNA and incubated for ~2 days before treating with PHA (2 h), harvesting for protein extraction and analysing by western blot for STIM1 and actin expression. (**B**–**H**) Jurkat cells transfected with scrambled RNA or STIM1 siRNA were treated with PHA or vehicle for 2 h before loading with fura-2 and depleting ER Ca^{2+} stores with Tg (2 μM). Subsequent elevation of $[Ca^{2+}]_e$ to 1 mM led to elevated $[Ca^{2+}]_c$; upon reaching its peak, $[Ca^{2+}]_e$ was again removed to monitor $[Ca^{2+}]_c$ clearance. Note that only the last part of each curve is depicted due to space considerations (except **E**). (**B**–**D**) Representative traces of $[Ca^{2+}]_c$ clearance in Jurkat cells after transfection with (**B**) scrambled RNA, (**C**) STIM1 siRNA or (**D**) in the presence of 300 nM BTP2 before and after treatment with PHA. Symbols represent individual data points while the solid lines are interpolated from non-linear regression analysis. (**E**) Representative traces of SOCe in Jurkat cells after transfection with scrambled RNA or STIM1 siRNA (Ctl or S1KD, respectively) or in the presence of 300 nM BTP2 (Ctl-BTP2 or PHA-BTP2, respectively). (**F**) Magnitude of SOCe from Ctl-BTP2 and PHA-BTP2 cells assessed by subtracting basal F_{340}/F_{380} from maximum F_{340}/F_{380} reached during the application of 1 mM extracellular Ca^{2+}. (**G**) The experiments depicted in (**B**) were fit to a two-phase non-linear decay curve (Ctl, $R^2 = 0.78$, $n = 5$; PHA, $R^2 = 0.78$, $n = 5$); half-lives depicted were analysed by the extra sum of squares *F*-test. * denotes statistically significant difference ($P < 0.05$). (**H**) The experiments depicted in (**C**, **D**) were fit to a one-phase non-linear decay curve (Ctl, $R^2 = 0.80$, $n = 5$; PHA, $R^2 = 0.85$, $n = 5$).

expression of shRNA-resistant YFP-tagged $STIM1_{wt}$ rescued PHA-dependent attenuation of PMCA-mediated Ca^{2+} clearance in shS1-expressing cells (Figure 6D). In contrast, transfecting cells with shRNA-resistant YFP-tagged $STIM1_{\Delta 597}$ failed to rescue PHA-dependent attenuation PMCA-mediated Ca^{2+} clearance in shS1 cells (Figure 6E). Importantly, both $STIM1_{wt}$ and $STIM1_{\Delta 597}$ reconstituted SOCe to similar levels in shS1 cells, highlighting that $STIM1_{\Delta 597}$ exhibits no defects in its ability to stimulate $[Ca^{2+}]_e$ entry (Figure 6F). Finally, coimmunoprecipitations were used to determine if the STIM1 truncation would affect STIM1–PMCA interaction. We found that both $STIM1_{wt}$ and $STIM1_{\Delta K}$ coprecipitated with endogenous PMCA, while $STIM1_{\Delta 597}$ did not (Figure 6G and H). Thus, whereas $STIM1_{\Delta 597}$ can functionally reorganize to close proximity of PMCA during cell activation, this protein either fails to bind to PMCA within this region or the stability of this interaction is significantly reduced. Nevertheless, these findings support the notion that the C-terminal domains of STIM1 are critical for PMCA modulation and provide strong support for the idea that a STIM1–PMCA interaction may account for decreased $[Ca^{2+}]_c$ clearance after PHA treatment.

Local control of Ca^{2+} entry and clearance at the IS

Throughout the course of our investigation, we consistently noted remarkable and wholly unexpected subcellular differences in *both* the entry and clearance of $[Ca^{2+}]_c$ in activated Jurkat cells. It has been noted in numerous studies that T cells polarize during activation (Kummerow *et al*, 2009); indeed, STIM1 has been shown to accumulate in both the IS and its opposing 'cap' upon activation (Barr *et al*, 2008; Lioudyno *et al*, 2008). In an effort to determine the relationship between these subcellular differences in Ca^{2+} concentration and these distinct areas of activated T cells, we examined cells activated using Alexafluor594-tagged PHA. Intriguingly, we found that these sites of PHA accumulation were the last areas of the cell to exhibit elevated $[Ca^{2+}]_c$ when the $[Ca^{2+}]_e$ was increased to 1 mM (Figure 7A; 10, 20, 22 s; Supplementary Figure S4A; Supplementary Movie 1) and the last areas of the cells to reach basal $[Ca^{2+}]_c$ when extracellular Ca^{2+} was removed (Figure 7A; 108, 112, 124 s; Supplementary Figure S4A; Supplementary Movie 1). Remarkably, S1KD dramatically altered this effect; while we still observed elevated $[Ca^{2+}]_c$ near the cap prior to the rest

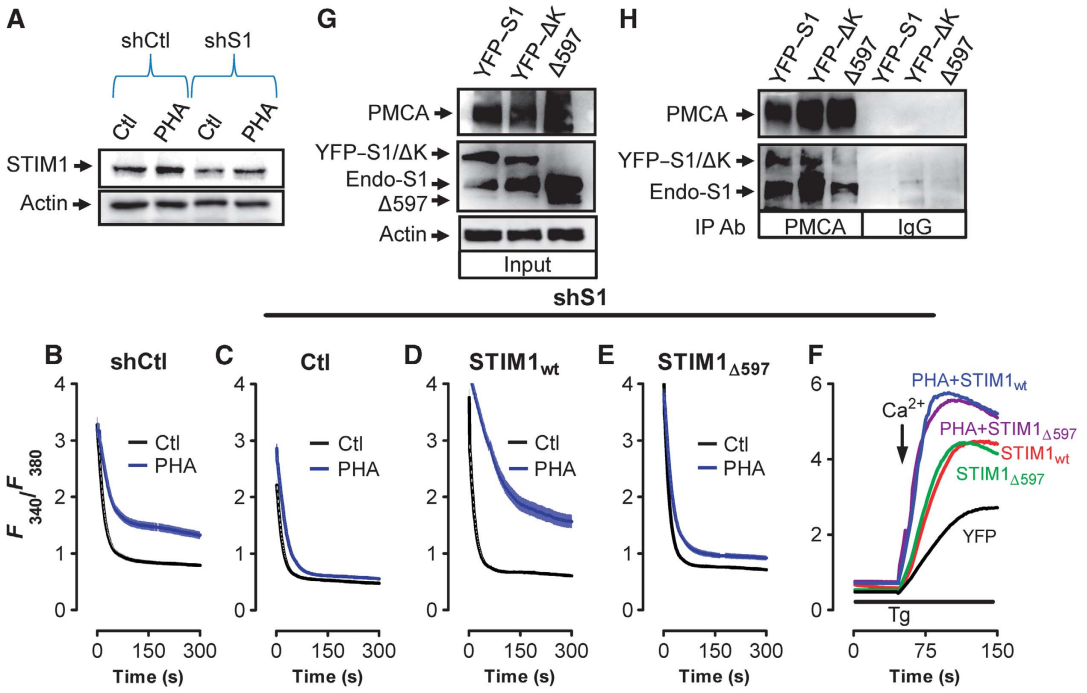

Figure 6 $STIM1_{wt}$ reconstitutes attenuation of PMCA during T-cell activation in S1KD cells. (**A**) Jurkat T cells stably expressing shCtl or shS1 were incubated ~2 days before treating with PHA (2 h), harvesting for protein extraction and analysing by western blot for STIM1 and actin expression. (**B–E**) Jurkat cells stably expressing shCtl (**B**) or shS1 (**C–E**) were transfected as indicated and treated with PHA or vehicle for 2 h before loading with fura-2 and depleting ER Ca^{2+} stores with Tg with Tg (2 μM). Subsequent elevation of $[Ca^{2+}]_e$ to 1 mM led to elevated $[Ca^{2+}]_c$; upon reaching its peak, $[Ca^{2+}]_e$ was again removed to monitor $[Ca^{2+}]_c$ clearance. Note that only the last part of each curve is depicted due to space considerations. Representative traces of $[Ca^{2+}]_c$ clearance experiments under each condition are shown. (**F**) Representative traces showing SOCe in Jurkat cells stably expressing shS1 and transiently transfected with YFP, $STIM1_{wt}$ or $STIM1_{\Delta597}$. (**G**, **H**) Jurkat cells were transfected with empty vector, $STIM1_{wt}$, $STIM1_{\Delta K}$ or $STIM1_{\Delta597}$ followed by lysis, and immunoprecipitation with PMCA or IgG antibodies (**G**) followed by western analysis. (**H**) In all, 25 μg of total protein was loaded to determine relative expression levels of STIM1 and PMCA prior to immunoprecipitation. Actin was used as a loading control.

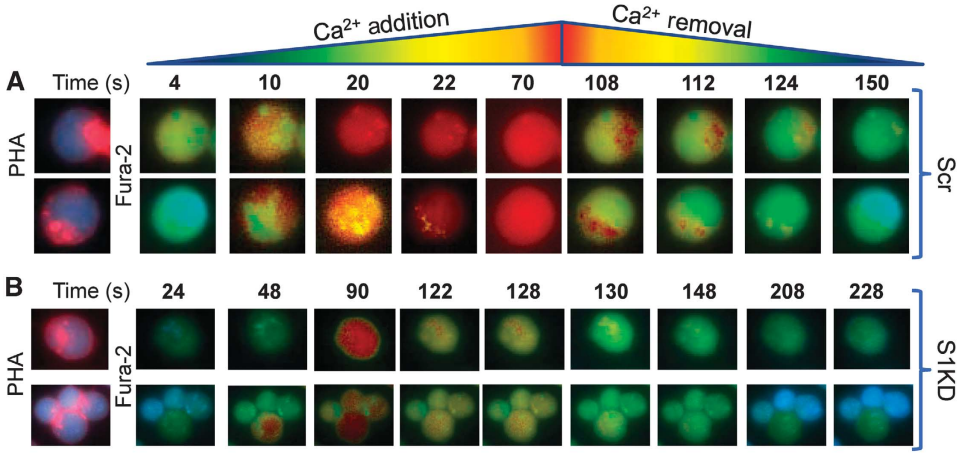

Figure 7 STIM1 and PMCA reorganize to the IS and regulate local Ca^{2+} signals. (**A**, **B**) Jurkat cells transfected with scrambled RNA (**A**) or STIM1 siRNA (**B**) were placed on cover slips, treated with 1 μg/ml Alexafluor594-conjugated PHA for 2 h followed by loading with Fura-2 and treating with Tg (2 μM). Localization of Alexafluor594-conjugated PHA is shown at the far left panel; all other images depict relative Fura-2 fluorescence (legend at the top) in the presence or absence of $[Ca^{2+}]_e$ (1 mM for wt; 10 mM for S1KD to increase cytosolic $[Ca^{2+}]_c$ to levels comparable to wt). Time points indicate time from addition of Ca^{2+}.

of the cell (Figure 7B; 48, 90 s; see Supplementary Figure S4B; Supplementary Movie 2), $[Ca^{2+}]_c$ started to decrease before extracellular Ca^{2+} was removed, with no apparent subcellular differences in $[Ca^{2+}]_c$ observed (Figure 7B; 122–228 s; see Supplementary Figure S4B; Supplementary Movie 2). Hence, these data indicate that inhibition of Ca^{2+} clearance may be restricted to the region of the cell immediately surrounding the synapse in activated cells, a concept supported by comparison of $[Ca^{2+}]_c$ clearance rates near the IS with those from the opposite end of the cell (Supplementary

Figure S5). Further, the fact that elevation of $[Ca^{2+}]_c$ was also delayed near the synapse may indicate that the association of STIM1 with PMCA decreases association between STIM1 and Orai1 in this region of the cell. If so, the net effect of restricting STIM1 and PMCA cytolocalization would be to elevate $[Ca^{2+}]_c$ in the peri-synaptic region while avoiding the complete disabling of cellular Ca^{2+} homeostasis.

Concluding remarks

The current investigation reveals a novel role for STIM1 as a modulator of $[Ca^{2+}]_c$ levels through regulation of PMCA-mediated $[Ca^{2+}]_c$ clearance. We conclude that both the upregulation and aggregation of STIM1 and PMCA to the region of the IS influences the spatial and temporal properties of Ca^{2+} signals, a concept supported by two investigations that were published while the current study was under review (Krapivinsky *et al*, 2011; Quintana *et al*, 2011). We propose that, at the IS, STIM1 attenuates PMCA-mediated $[Ca^{2+}]_c$ clearance, which may occur through a conformational coupling mechanism analogous to that used by STIM1 to activate Orai1. Our conclusions are drawn from strong functional evidence showing that (a) overexpression of STIM1 alone attenuates PMCA-mediated Ca^{2+} clearance, (b) attenuation of PMCA-mediated $[Ca^{2+}]_c$ clearance during T-cell activation is absent after STIM1 knockdown and (c) the ability of STIM1 to mediate Orai1 activation could be separated from its ability to inhibit PMCA activity by mutational analysis.

It is noteworthy that the correlation between STIM1 expression and inhibition of Ca^{2+} clearance was non-linear. Hence, the extent to which $[Ca^{2+}]_c$ clearance was inhibited after ectopic expression of YFP–STIM1 or activation by PHA was similar, despite marked differences in STIM1 expression levels. Further, PHA-induced inhibition of $[Ca^{2+}]_c$ clearance could be completely eliminated by a 50% reduction in STIM1 expression after knockdown by shRNA. While the latter observation is consistent with the existence of a threshold requirement for STIM1 for regulation of $[Ca^{2+}]_c$ clearance, the former may reflect the involvement of additional players in this process (such as POST (Krapivinsky *et al*, 2011) and others).

That we observe these events occurring during T-cell activation seems fitting since there is substantial evidence that elevated Ca^{2+} signals are required for NFAT activation and subsequent cytokine production during T-cell activation. Whereas the requirement of STIM1 to activate NFAT during T-cell activation is now well established (Oh-Hora *et al*, 2008), our findings provide an additional role for STIM1 in this process via local modulation of PMCA function to enhance NFAT activity in the peri-synaptic area. This function may be further supported by the previously reported ability of PMCA to serve as a scaffold for calcineurin (Buch *et al*, 2005), the effector of NFAT activation. Finally, the current study reveals PMCA as a member of a growing list of STIM1 targets that include members of the Orai (Mercer *et al*, 2006; Peinelt *et al*, 2006; Soboloff *et al*, 2006) and TRPC (Ong *et al*, 2007; Worley *et al*, 2007; Yuan *et al*, 2007) families, adenylate cyclases (Lefkimmiatis *et al*, 2009) and CaV1.2 (Park *et al*, 2010; Wang *et al*, 2010). Given the relatively wide expression of STIM1 and how few of its many distinct domains are now understood, future studies directed at other potential targets may be revealing.

Materials and methods

Cell culture

Jurkat (ATCC) and CEM391 (generously provided by Dr Ana Gamero, Temple University) T cells along with freshly collected primary thymocytes were cultured in RPMI supplemented with 10% FBS and antibiotics. All cells were maintained at 37°C; 5% CO_2.

Cytosolic Ca^{2+} measurements

Cells were plated on coverslips and placed in cation-safe solution (107 mM NaCl, 7.2 mM KCl, 1.2 mM $MgCl_2$, 11.5 mM glucose, 20 mM Hepes-NaOH, 1 mM $CaCl_2$, pH 7.2) and loaded with fura-2/acetoxymethylester (2 μM) for 30 min at 24°C. Cells were washed, and dye was allowed to de-esterify for a minimum of 30 min at 24°C. Approximately 85% of the dye was confined to the cytoplasmas determined by the signal remaining after saponin permeabilization. Ca^{2+} measurements were made using a Leica DMI 6000B fluorescence microscope controlled by Slidebook Software (Intelligent Imaging Innovations; Denver, CO). Fluorescence emission at 505 nm was monitored while alternating between 340 and 380 nm excitation wavelengths at a frequency of 0.67 Hz; intracellular Ca^{2+} measurements are shown as 340/380 nm ratios obtained from groups (35–45) of single cells. In all experiments depicting PHA-mediated T-cell activation, 1 μg/ml PHA was added to cells for 2 h. Cells were cultured in serum-free medium containing 0.5% BSA for 12 h prior to the addition of PHA or vehicle. To both induce SOCe and measure PMCA-mediated Ca^{2+} clearance, the function of SERCA was inhibited by the addition of Tg (2 μM). Ca^{2+} was added after recovery of cytosolic Ca^{2+} content and then removed once peak levels had been reached to measure Ca^{2+} clearance.

Mitochondrial Ca^{2+} measurements

Cells were placed on coverslips in RPMI medium containing 10 μM rhod-2 AM (Invitrogen) and incubated at 37°C, 5% CO_2 for 1 h. Coverslips were then removed from the incubator and loaded with Fura-2 (as described above) in order to monitor cytosolic and mitochondrial Ca^{2+} signals simultaneously. For inhibition of mitochondrial Ca^{2+} uptake, 10 μM Ru360 (Invitrogen) was added to the cation-safe solution during Fura-2 dye loading in order to achieve a 1-h treatment with the inhibitor prior to Ca^{2+} measurements; Ru360 was maintained in the imaging buffer throughout the entire Ca^{2+} measurement to avoid Ru360 wash out. Mitochondrial Ca^{2+} measurements were made using a Leica DMI 6000B fluorescence microscope controlled by Slidebook Software (Intelligent Imaging Innovations; Denver, CO). For rhod-2 measurements, fluorescence emission at 605 nm was monitored after 546 nm excitation at a frequency of 0.67 Hz.

Cell lysis and western blot

Cells were lysed in CHAPS lysis buffer (35 mM CHAPS, 150 mM NaCl, 100 mM Tris–HCl, 10 mM EDTA pH 8.0 with protease inhibitors), cleared by centrifugation and normalized for protein content (determined using the DC protein assay kit; Bio-Rad). Proteins were resolved on 6–8% SDS–PAGE gels transferred to nitrocellulose paper and analysed with the indicated antibodies as previously described.

Immunoprecipitation

Protein G beads (Invitrogen) were incubated with primary antibodies (mouse anti-PMCA, 10 μg; mouse anti-GOK, 10 μg; mouse anti-IgG 10 μg) for 1 h followed by overnight incubation with cell lysates (300 μg; 4°C). Beads were then washed three times with RIPA buffer followed by elution in sample buffer containing 5% β-mercaptoethanol for 10 min at 100°C.

Quantitative PCR

RNA was extracted using TRI Reagent (MRC). Briefly, 1 ml of TRI reagent was added per 10 cm culture dish. Homogenate was stored at room temperature for 5 min followed by the addition of 0.2 ml chloroform to allow for phase separation. The mixture was incubated at room temperature for 10 min and then centrifuged at 4°C at 12 000 **g** for 15 min. Aqueous phase was removed and mixed with 0.5 ml ethanol followed by centrifugation at 4°C at 12 000 **g** for 15 min to allow for RNA precipitation. RT–PCR was completed as a two-step process using High Capacity cDNA Reverse Transcription

(Applied Biosystems) followed by Sybr Green PCR (Applied Biosystems) on a 7300 Real-Time PCR machine (Applied Biosystems). The real-time reaction was carried out by a 10-min incubation at 95°C and 40 cycles at 95°C for 15 s and 60°C 1 min for annealing. Data are presented as a level relative to Tata-box-binding protein (TBP) using the following equation and primers:

PMCA 1
Sense 5′ -TAAGGGTGGTGGACTATCT-3′
Antisense 5′-TATTCCCTATGCCTTGTG-3′
PMCA4
Sense 5′-GTTCTCCATCATCCGAAACGG-3′
Antisense 5′-CAAGCATCCAAGTGCCGTACTAG-3′
TBP
Sense 5′-CAGCCGTTCAGCAGTCAA-3′
Antisense 5′-GGAGGGATACAGTGGAGT-3′

Materials

Peptide affinity-purified specific antibodies to STIM1 (input and time course studies) and STIM2 were produced by 21st Century Biochemicals (Marlboro, MA). Anti-GOK (for co-IP) was obtained from BD Biosciences (San Diego, CA). Anti-PMCA1,4 and anti-EGR1 were from Cell Signaling (Danvers, MA). PMCA4-specific antibodies were from Novus Biologicals (Littleton, CO). Fura-2/acetoxymethylester, Rhod-2, RU360.horseradish peroxidase-conjugated goat anti-rabbit and rabbit anti-mouse antibodies were obtained from Invitrogen (CA). Tg was obtained from EMD Biosciences (San Diego, CA). Untagged PHA was obtained from Sigma (St Louis, MO); Alexafluor594-tagged PHA was obtained from Invitrogen (Carlsbad, CA). The OKT3 monoclonal anti-CD3 antibody was obtained from Abcam (Cambridge, MA).

Plasmids

cDNAs encoding eYFP-tagged human STIM1 (YFP–STIM1) and eYFP-tagged human STIM2 (YFP–STIM2) were generated as previously described (Zhou *et al*, 2009). cDNAs encoding mCherry-STIM1 were obtained from Dr Muniswamy Madesh (Temple University). cDNAs encoding CFP–STIM1 were obtained from Dr Roger Tsien (UCSD) as previously described (Hauser and Tsien, 2007). STIM1 deletion constructs were obtained from Dr Marie Dziadek (Garvan Institute, Australia). $STIM1_{\Delta K}$ exhibits a deletion at aa 666 and the $STIM1_{\Delta 597}$ truncation is at aa 597. The shRNA-resistant YFP–$STIM1_{wt}$ plasmid was generated by site-directed mutagenesis (TGCCTATATC→cGCtTAcATa) of YFP–STIM1; this construct was then truncated at aa 597 to generate the shRNA-resistant YFP–$STIM1_{\Delta 597}$ construct (Mutagenex). YFP–$STIM1_{\Delta P}$ was generated by deleting amino acids 597–629 from YFP–STIM1 (Mutagenex). GFP–STIM1-NN was generously donated by Dr Anna Akhmonova; Erasmus Medical Center; The Netherlands. GFP–PMCA4b was obtained from Dr Emanuel Strehler (Mayo Clinic, Rochester, MN). CFP–PMCA4b was generated by cloning PMCA4b from GFP–PMCA4b and inserting it immediately after CFP within a pIRESneo vector (Mutagenex). Human STIM1 Stealth siRNA (Invitrogen) was targeted to position 3123 and had the sequence 5′-GGGCCUAAUCUUUGAAGUUUGUUCU-3′. Medium GC-rich RNAi control (Invitrogen) was used as a scrambled sequence. Human STIM1 shRNA (targeted to position 797; 5′-GATGATGCCAATGGTG ATGTGGATGTGGA-3) and scrambled control shRNA (Cat #TR30012) were obtained from Origene (Rockville, MD).

Supplementary data

Supplementary data are available at *The EMBO Journal* Online (http://www.embojournal.org).

Acknowledgements

We thank Dr Emanuel Strehler (Mayo Clinic, Rochester, MN), Dr Marie Dziadek (Garvan Institute, Australia), Dr Roger Tsien (UCSD), Dr Anna Akhmonova (Erasmus Medical Center; The Netherlands) and Dr Muniswamy Madesh (Temple University) for their valuable contributions of critical reagents in support of our project. We also thank Dr Donald Gill for his critical review of our data. This work was supported by NIH Grant #1R01GM097335-01A1 (JS).

Author contribution: MFR performed and designed the experiments, analysed the data and contributed to the writing of the manuscript. ES performed the experiments and analysed data. JS performed and designed the experiments, analysed the data and wrote the manuscript.

Conflict of interest

The authors declare that they have no conflict of interest.

References

Barr VA, Bernot KM, Srikanth S, Gwack Y, Balagopalan L, Regan CK, Helman DJ, Sommers CL, Oh-Hora M, Rao A, Samelson LE (2008) Dynamic movement of the calcium sensor STIM1 and the calcium channel Orai1 in activated T-cells: puncta and distal caps. *Mol Biol Cell* **19:** 2802–2817

Baughman JM, Perocchi F, Girgis HS, Plovanich M, Belcher-Timme CA, Sancak Y, Bao XR, Strittmatter L, Goldberger O, Bogorad RL, Koteliansky V, Mootha VK (2011) Integrative genomics identifies MCU as an essential component of the mitochondrial calcium uniporter. *Nature* **476:** 341–345

Bautista DM, Hoth M, Lewis RS (2002) Enhancement of calcium signalling dynamics and stability by delayed modulation of the plasma-membrane calcium-ATPase in human T cells. *J Physiol* **541:** 877–894

Bautista DM, Lewis RS (2004) Modulation of plasma membrane calcium-ATPase activity by local calcium microdomains near CRAC channels in human T cells. *J Physiol* **556:** 805–817

Buch MH, Pickard A, Rodriguez A, Gillies S, Maass AH, Emerson M, Cartwright EJ, Williams JC, Oceandy D, Redondo JM, Neyses L, Armesilla AL (2005) The sarcolemmal calcium pump inhibits the calcineurin/nuclear factor of activated T-cell pathway via interaction with the calcineurin A catalytic subunit. *J Biol Chem* **280:** 29479–29487

Caride AJ, Filoteo AG, Penheiter AR, Paszty K, Enyedi A, Penniston JT (2001) Delayed activation of the plasma membrane calcium pump by a sudden increase in Ca^{2+}: fast pumps reside in fast cells. *Cell Calcium* **30:** 49–57

Deng X, Wang Y, Zhou Y, Soboloff J, Gill DL (2009) STIM and Orai: dynamic intermembrane coupling to control cellular calcium signals. *J Biol Chem* **284:** 22501–22505

Di Capite J, Ng SW, Parekh AB (2009) Decoding of cytoplasmic Ca(2+) oscillations through the spatial signature drives gene expression. *Curr Biol* **19:** 853–858

Grigoriev I, Gouveia SM, van der Vaart B, Demmers J, Smyth JT, Honnappa S, Splinter D, Steinmetz MO, Putney Jr JW, Hoogenraad CC, Akhmanova A (2008) STIM1 is a MT-plus-end-tracking protein involved in remodeling of the ER. *Curr Biol* **18:** 177–182

Hauser CT, Tsien RY (2007) A hexahistidine-Zn^{2+}-dye label reveals STIM1 surface exposure. *Proc Natl Acad Sci USA* **104:** 3693–3697

He LP, Hewavitharana T, Soboloff J, Spassova MA, Gill DL (2005) A functional link between store-operated and TRPC channels revealed by the 3,5-bis(trifluoromethyl)pyrazole derivative, BTP2. *J Biol Chem* **280:** 10997–11006

Hogan PG, Lewis RS, Rao A (2010) Molecular basis of calcium signaling in lymphocytes: STIM and ORAI. *Ann Rev Immunol* **28:** 491–533

Honnappa S, Gouveia SM, Weisbrich A, Damberger FF, Bhavesh NS, Jawhari H, Grigoriev I, van Rijssel FJ, Buey RM, Lawera A, Jelesarov I, Winkler FK, Wuthrich K, Akhmanova A, Steinmetz MO (2009) An EB1-binding motif acts as a microtubule tip localization signal. *Cell* **138:** 366–376

Ishikawa J, Ohga K, Yoshino T, Takezawa R, Ichikawa A, Kubota H, Yamada T (2003) A pyrazole derivative, YM-58483, potently inhibits store-operated sustained Ca^{2+} influx and IL-2 production in T lymphocytes. *J Immunol* **170:** 4441–4449

Krapivinsky G, Krapivinsky L, Stotz SC, Manasian Y, Clapham DE (2011) POST, partner of stromal interaction molecule 1 (STIM1), targets STIM1 to multiple transporters. *Proc Natl Acad Sci USA* **108:** 19234–19239

Kummerow C, Junker C, Kruse K, Rieger H, Quintana A, Hoth M (2009) The immunological synapse controls local and global calcium signals in T lymphocytes. *Immunol Rev* **231:** 132–147

Lefkimmiatis K, Srikanthan M, Maiellaro I, Moyer MP, Curci S, Hofer AM (2009) Store-operated cyclic AMP signalling mediated by STIM1. *Nat Cell Biol* **11:** 433–442

Lewis RS (2001) Calcium signaling mechanisms in T lymphocytes. *Ann Rev Immunol* **19:** 497–521

Lioudyno MI, Kozak JA, Penna A, Safrina O, Zhang SL, Sen D, Roos J, Stauderman KA, Cahalan MD (2008) Orai1 and STIM1 move to the immunological synapse and are up-regulated during T cell activation. *Proc Natl Acad Sci USA* **105:** 2011–2016

Mercer JC, Dehaven WI, Smyth JT, Wedel B, Boyles RR, Bird GS, Putney Jr JW (2006) Large store-operated calcium selective currents due to co-expression of Orai1 or Orai2 with the intracellular calcium sensor, Stim1. *J Biol Chem* **281:** 24979–24990

Oh-hora M (2009) Calcium signaling in the development and function of T-lineage cells. *Immunol Rev* **231:** 210–224

Oh-hora M, Rao A (2008) Calcium signaling in lymphocytes. *Curr Opin Immunol* **20:** 250–258

Oh-Hora M, Yamashita M, Hogan PG, Sharma S, Lamperti E, Chung W, Prakriya M, Feske S, Rao A (2008) Dual functions for the endoplasmic reticulum calcium sensors STIM1 and STIM2 in T cell activation and tolerance. *Nat Immunol* **9:** 432–443

Ong HL, Cheng KT, Liu X, Bandyopadhyay BC, Paria BC, Soboloff J, Pani B, Gwack Y, Srikanth S, Singh BB, Gill D, Ambudkar IS (2007) Dynamic assembly of TRPC1-STIM1-Orai1 ternary complex is involved in store-operated calcium influx. Evidence for similarities in store-operated and calcium release-activated calcium channel components. *J Biol Chem* **282:** 9105–9116

Park CY, Shcheglovitov A, Dolmetsch R (2010) The CRAC channel activator STIM1 binds and inhibits L-type voltage-gated calcium channels. *Science* **330:** 101–105

Peinelt C, Vig M, Koomoa DL, Beck A, Nadler MJ, Koblan-Huberson M, Lis A, Fleig A, Penner R, Kinet JP (2006) Amplification of CRAC current by STIM1 and CRACM1 (Orai1). *Nat Cell Biol* **8:** 771–773

Quintana A, Pasche M, Junker C, Al-Ansary D, Rieger H, Kummerow C, Nunez L, Villalobos C, Meraner P, Becherer U, Rettig J, Niemeyer BA, Hoth M (2011) Calcium microdomains at the immunological synapse: how ORAI channels, mitochondria and calcium pumps generate local calcium signals for efficient T-cell activation. *EMBO J* **30:** 3895–3912

Quintana A, Schwarz EC, Schwindling C, Lipp P, Kaestner L, Hoth M (2006) Sustained activity of calcium release-activated calcium channels requires translocation of mitochondria to the plasma membrane. *J Biol Chem* **281:** 40302–40309

Quintana A, Schwindling C, Wenning AS, Becherer U, Rettig J, Schwarz EC, Hoth M (2007) T cell activation requires mitochondrial translocation to the immunological synapse. *Proc Natl Acad Sci USA* **104:** 14418–14423

Reicher B, Barda-Saad M (2010) Multiple pathways leading from the T-cell antigen receptor to the actin cytoskeleton network. *FEBS Lett* **584:** 4858–4864

Ritchie MF, Yue C, Zhou Y, Houghton PJ, Soboloff J (2010) Wilms tumor suppressor 1 (WT1) and early growth response 1 (EGR1) are regulators of STIM1 expression. *J Biol Chem* **285:** 10591–10596

Schwindling C, Quintana A, Krause E, Hoth M (2010) Mitochondria positioning controls local calcium influx in T cells. *J Immunol* **184:** 184–190

Soboloff J, Spassova MA, Tang XD, Hewavitharana T, Xu W, Gill DL (2006) Orai1 and STIM reconstitute store-operated calcium channel function. *J Biol Chem* **281:** 20661–20665

Wang Y, Deng X, Mancarella S, Hendron E, Eguchi S, Soboloff J, Tang XD, Gill DL (2010) The calcium store sensor, STIM1, reciprocally controls Orai and CaV1.2 channels. *Science* **330:** 105–109

Worley PF, Zeng W, Huang GN, Yuan JP, Kim JY, Lee MG, Muallem S (2007) TRPC channels as STIM1-regulated store-operated channels. *Cell Calcium* **42:** 205–211

Yuan JP, Zeng W, Huang GN, Worley PF, Muallem S (2007) STIM1 heteromultimerizes TRPC channels to determine their function as store-operated channels. *Nat Cell Biol* **9:** 636–645

Zhou Y, Mancarella S, Wang Y, Yue C, Ritchie M, Gill DL, Soboloff J (2009) The short N-terminal domains of STIM1 and STIM2 control the activation kinetics of Orai1 channels. *J Biol Chem* **284:** 19164–19168

Zitt C, Strauss B, Schwarz EC, Spaeth N, Rast G, Hatzelmann A, Hoth M (2004) Potent inhibition of Ca^{2+} release-activated Ca^{2+} channels and T-lymphocyte activation by the pyrazole derivative BTP2. *J Biol Chem* **279:** 12427–12437